Characterization of the Dizinc Analogue of the Synthetic Diiron Protein DF1 Using ab Initio and Hybrid Quantum/Classical Molecular Dynamics Simulations

Alessandra Magistrato,*,† William F. DeGrado,‡ Alessandro Laio,§ Ursula Rothlisberger,|| Joost VandeVondele,⊥ and Michael L. Klein†

Center for Molecular Modeling, Department of Chemistry, University of Pennsylvania, Philadelphia, Pennsylvania 19104-6323, Department of Biochemistry and Biophysics, University of Pennsylvania, School of Medicine, Philadelphia, Pennsylvania 19104-6054, CSCS, CH-6928 Manno, Switzerland, Institute of Molecular Chemistry and Biology, EPFL, CH-1025 Lausanne, Switzerland, and Laboratory for Physical Chemistry, University of Zürich CH-8057, Zürich, Switzerland

Received: September 19, 2002; In Final Form: February 11, 2003

The structural and dynamical properties of the four α-helix bundle Due Ferri 1, which is a generic mimic of diiron proteins, have been explored using density functional theory (DFT) based and hybrid quantum/classical molecular dynamics (QM/MM) simulations. Four quantum mechanical (QM) representations of the active site have been employed in order to systematically assess the role of first and second shell interactions: (a) a 66-atom fragment of the active site comprising only first shell ligands, (b and c) two systems (78 and 86 atoms) containing different second shell hydrogen bonds, and (d) a 98-atom model including both the first and second shell residues. Two QM/MM partitioning schemes have been explored in order to explicitly consider the role of the whole protein environment: (a) a 54-QM-atom model in which only the first shell ligands are described at the DFT level, while the rest of the protein environment is taken into account at the MM level and (b) a 68-QM-atom model in which the first shell ligands plus a second shell hydrogen bond network is considered at the DFT level. All of the calculations confirm the highly flexible nature of the carboxylate-bridged binuclear motif and demonstrate the importance of the whole protein environment in stabilizing the hydrogen bond networks that surround the active site. The present QM/MM approach allows for the identification of key factors governing the stability/reactivity of the active site and thus provides unique insights that can be exploited for the future tailoring of new highly selective biomimetic enzymatic compounds.

1. Introduction

Proteins utilize a limited repertoire of metal ions and metal binding sites to catalyze a multitude of different chemical reactions. For example, diiron proteins[1] with similar active sites promote reversible oxygen binding and activation;[2] oxygen transport;[3] hydroxylation of alkane,[1,2] alkene, and aromatic groups;[4] epoxidation;[5] desaturation;[6] and the formation of organic radicals.[7] A complete understanding of how proteins tune a common diiron active site in order to obtain a variety of highly specific catalysts is far from trivial.[1−7]

Among the diiron enzymes, a key role is played by methane monooxygenase (MMO), which catalyzes the conversion of the inert molecule methane to methanol.[4] This reaction occurs in nature under mild conditions and in an efficient and highly selective manner,[1,2] while the corresponding industrial process occurs under extreme conditions with low yields.[8,9] Thus, the idea of synthesizing enzyme mimics emerges quite naturally. However, the search for synthetic molecules capable of reproducing biological processes presents a challenge, since the knowledge of enzymatic mechanisms is often hampered by their complexity. Indeed, few model compounds exist[10] that reproduce the carboxylate bridged binuclear motif that is at the core of the MMO active site. Such complexes have proven to be invaluable complements to crystal,[11] spectroscopic,[1,2,12] and theoretical data[13] for understanding the structure and stability of possible catalytic intermediates.

Recently, a four α-helix peptide bundle that mimics the structural features common to this class of diiron proteins has been synthesized and characterized.[14−16] This synthetic biomimetic complex (Figure 1), named Due Ferro 1 (DF1), has been realized by performing a retro structural analysis[14−16] of a series of ferroxidases (ferritin,[17] bacterioferritin,[18] and rubrerythrin[19]), ribonucleotide reductase R2 subunit,[20] Δ9 ACP desaturase,[21] and the catalytic subunit of MMO.[1,2,4,11−13] The complex is formed by four antiparallel α-helices with four Glu residues that project toward the center of the bundle to form the active site. Two of the Glu residues bridge both metal ions, whereas the other two carboxylates interact with a single metal ion in a monodentate or bidentate chelating interaction. Two histidine residues, coming from two different helices, form additional monodentate ligands.

A four α-helix peptide bundle such as DF1 presents a number of distinct advantages with respect to typical small synthetic mimics of metalloproteins.[10] In fact, DF1 not only addresses the question of how the arrangement of atoms in the active site leads to function but also emulates the tertiary structure of the real enzymes. In addition, DF1 binds different metal ions[14−16] such as zinc, cobalt, manganese, and iron, thus becoming

* Corresponding author. E-mail: ale@cmm.upenn.edu.
† Center for Molecular Modeling.
‡ Department of Biochemistry and Biophysics.
§ CSCS.
|| Institute of Molecular Chemistry and Biology.
⊥ Laboratory for Physical Chemistry.

10.1021/jp027032o CCC: $25.00 © 2003 American Chemical Society
Published on Web 04/02/2003

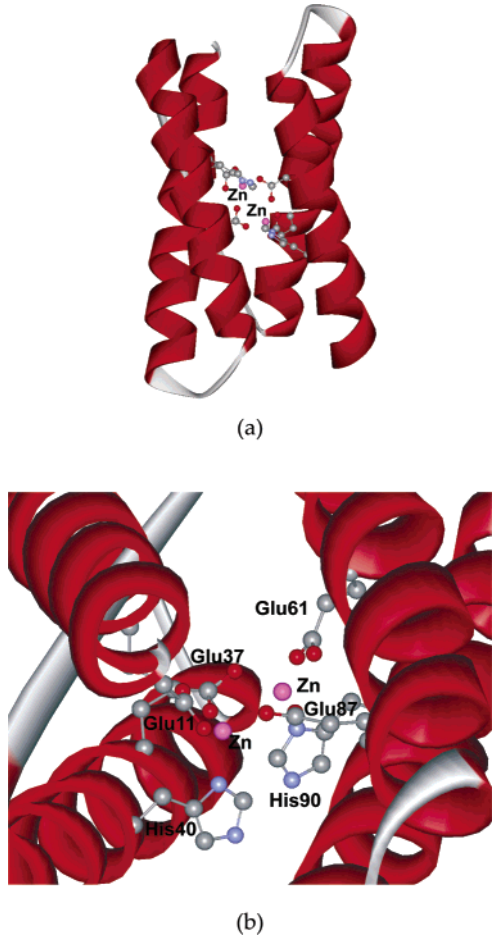

Figure 1. (a) Schematic structure of the four-helix bundle biomimetic compound DF1. (b) Closer view of the bridged bimetallic putative catalytic center.

potentially able to catalyze a multitude of important chemical reactions promoted not only by diiron proteins[1−7] but also by dizinc (e.g., amino peptidase[21−23]) and dimanganese (e.g., manganese catalase,[24−26] arginase,[24,27] bis-Mn(II) R2[28]) containing enzymes. All these proteins share with DF1 the same carboxylate bridged binuclear motif. Thus, the study of the biomimetic compound DF1, and its dimetal analogues, could provide an invaluable complement to spectroscopic and structural data available on the aforementioned real enzymes. Clearly, a biomimetic complex able to perform oxygen activation processes under mild conditions would solve issues of considerable scientific and economic relevance.[9] However, to date, an effective tailoring of DF1 is hampered by the lack of detailed structural and dynamical information about the active site and the specific role of the various second shell ligands.[14−16]

Due to the crucial chemical and biological relevance of carboxylate bridged binuclear proteins, we present here a structural and dynamical characterization of the dizinc analogue of DF1 through first-principles (Car−Parrinello)[29] and hybrid QM/MM molecular dynamic simulations. This method is particularly suited for the study of complex biological systems[30] since it allows one to model the systems considering explicitly the entire molecular structure and solvent effects. In fact, by including the active site of the enzyme in the quantum mechanical (QM) region we can provide an accurate description of the core of the enzyme, while the rest of the protein can be described by molecular dynamics based on standard force fields.

In this article, we report the results of a systematic theoretical study on the dizinc analogue of DF1, using a variety of QM and QM/MM partitioning schemes, to elucidate the key factors governing stability/reactivity of the active site. The present work indicates that the dynamical features of the carboxylate bridged binuclear motif need to be explored while the entire protein environment along with the solvent water are simultaneously being taken explicitly into account. Such studies will be critically important for the future tailoring of efficient and highly selective biomimetic catalysts.

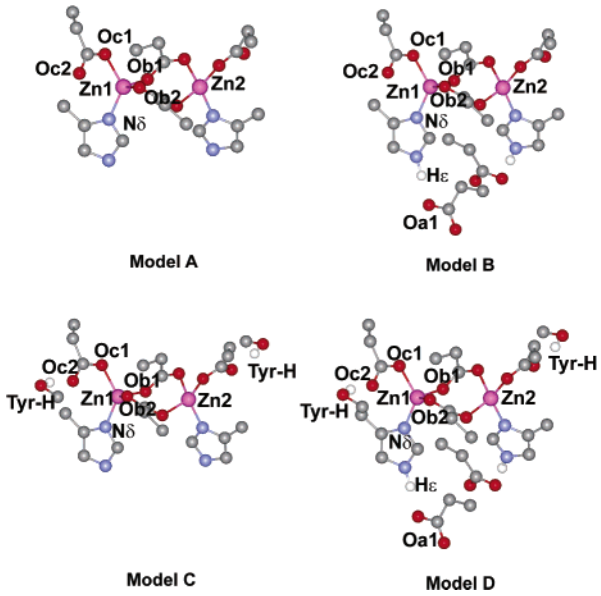

Figure 2. Quantum mechanical models of the active site of DF1.

2. Computational Details

In the first part of this work, the focus is on the active site region of DF1. First-principles molecular dynamics (Car−Parrinello)[29,31] simulations have been performed on four different QM fragments representing the active site (Figure 2). Model A (Figure 2a) involves two zinc ions and the residues directly coordinated to them: two bridging carboxylate ligands (Glu37 and Glu87), two chelating carboxylates (Glu11 and Glu61), and two histidines (His40 and His90). All of the amino acid residues have been cut at the β-carbon, and the C(β) valence has been saturated with hydrogen atoms. In model B (Figure 2b), the influence of two second shell ligands on the structural properties of the active site is considered by adding two aspartate residues (Asp36 and Asp86) to the ligands considered in model A. This allows for the inclusion of the hydrogen bonds between aspartates and histidines.[14−16] Aspartates have been cut at C(α), and for this (and for the following computational models), all the terminal carbons have been fixed at their crystallographic positions. A third representation (model C in Figure 2c) has been chosen in order to emulate a different kind of second shell interaction (i.e., a hydrogen bond between oxygen of the chelating carboxylates (Oc2) and a tyrosine residue (Tyr18 and Tyr78)). Due to the large size of the tyrosine residue, a computational model comprehensive of the whole side chain would lead to a prohibitively large computational effort. Therefore, for a qualitative estimation of the role of this hydrogen bond network, we simply replace the tyrosine side chain with a methanol molecule. The *para*-carbon of the aromatic ring has been constrained to the original position it occupied in the X-ray structure, and its valence has been saturated with hydrogen atoms. Finally, we have considered a model encompassing all first and second shell ligands (model D, Figure 2d).

All calculations were performed with the program CPMD,[32] which is an implementation of the original Car−Parrinello scheme, based on density functional theory (DFT), periodic boundary conditions, a plane wave basis set, and a pseudopotential formalism. An analytical pseudopotential was used for hydrogen and a nonlocal, norm-conserving soft pseudopotential of the Martins−Trouiller type[33] for all the other elements. Angular momentum components with $l_{max} = 1$ have been included for carbon, nitrogen, and oxygen. For zinc, we used a pseudopotential with cutoff radii $r_s = 1.8$ au, $r_p = 2.0$ au, $r_d = 1.8$ au, and $r_f = 1.2$ au which incorporates also scalar relativistic effects. All pseudopotentials have been transformed to a fully nonlocal form using the scheme developed by Kleinman and Bylander[34] whereas for zinc, the nonlocal part of the pseudopotential has been integrated numerically using a Gauss−Hermite quadrature. This setup has been shown to accurately describe the Zn(II) sites in the enzyme carbonic anhydrase[35] and alcohol dehydrogenase[36] and β-lactamase.[37] All results presented here have been obtained using a kinetic energy cutoff of 70 Ry. The gradient corrected scheme developed by Becke (B)[38] and by Lee, Yang, and Parr (LYP)[39] was used to describe the exchange and the correlation part, respectively. This exchange−correlation functional has been shown to describe accurately the structure and the bonding of a variety of enzymatic systems.[40] Calculations were performed in an orthorhombic box with edges of $a = 16$ Å, $b = 15$ Å, and $c = 17$ Å for model A and $a = 16.5$ Å, $b = 18.5$ Å, $c = 20.6$ Å for models B, C, and D, respectively. For all models, periodic images were decoupled using the scheme of Hockney.[41]

In the QM/MM calculations, the system has been partitioned into two regions: one treated at a QM-DFT level using CPMD and the other at the MM level using a classical force field. Two different partitioning schemes have been adopted for these hybrid calculations. In model 1 (Figure 3a), the QM region comprises the active site of the enzyme, including the two zinc atoms, two bridging carboxylate ligands (Glu37 and Glu87), two chelating carboxylates (Glu11 and Glu61), plus two histidines (His40 and His90). The side chains of the animo acids in the QM region have been cut at the C(α) and C(β), for the histidine and the carboxylate side chains, respectively. All other atoms have been treated at the MM level. In the second QM/MM model (model 2, in Figure 3b), in addition to the residues of model 1, we also include in the QM part two aspartate side chains (Asp36 and Asp86). The aspartate side chains are cut at the C(α). The Cα−Cβ bonds cross the QM/MM interface for Glu37, Glu87, Glu11, Glu71, His40, and His90, while for Asp36 and Asp86, the Cα−C bond is at the boundary between the QM and the MM region. For both QM/MM models we have replaced the terminal carbons (Cβ for Glu and His residues and Cα for Asp residues) with dummy pseudopotentials that mimic the electronic properties of a methyl group.[42]

Initially, the whole system (four-helix bundle plus a shell of 9 Å of solvent waters) was equilibrated by performing purely classical molecular dynamics using the Amber 6 package.[43] The TIP3P model[43] has been used to treat the solvent water molecules. Constant NVT simulations were performed by coupling the system to a thermostat[43] in order to equilibrate hydrogen atoms and solvent molecules, while the rest of the protein was kept fixed. Then, the entire structure was equilibrated using a time step of 1 fs with all the bond lengths fixed by applying a SHAKE algorithm.[44] Using this protocol, NPT dynamics was performed for 500 ps. During this equilibration, restraints were applied to the Zn−Zn distance and to the distances between the zincs and the oxygens of the bridging and chelating carboxylates.

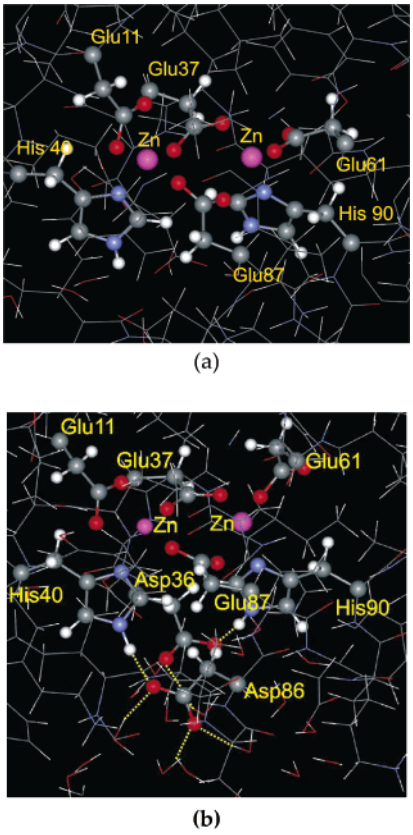

Figure 3. (a) QM/MM model 1 and (b) model 2. Atoms drawn in ball-and-stick are included in the QM region; atoms in stick only are included in the MM region. (b) View of the hydrogen bond network involving the putative active site of DF1, second shell ligands, and water molecules.

In the two QM/MM studies, DFT-based CPMD calculations were carried out at 300 K with a time step of 4 au using a fictitious electronic mass of $\mu = 800$ au. Orthorhombic boxes with dimensions $a = 15.5$ Å, $b = 19$ Å, and $c = 19.5$ Å and $a = 15.5$ Å, $b = 20$ Å, $c = 21$ Å were employed for models 1 and 2, respectively. Periodic images have been decoupled.[41] The electrostatic interactions between the quantum and classical regions of the system were handled via a fully Hamiltonian coupling scheme.[45] In this approach, the short range electrostatic interactions between the QM and the MM part of the system are explicitly taken into account within a sphere of radius 5.3 Å around every QM atom, using an appropriately modified Coulomb potential that ensures that no electron spill-out[45,46] occurs. The electrostatic interactions with the more distant MM atoms are treated with a multipole expansion for the QM region. Bonded and van der Waals interactions between the QM and the MM part are treated with the standard Amber force field.[43] Further details of the mixed QM/MM method used in this work are given in ref 45. Long-range electrostatic interactions between MM atoms have been described with P3M implementation.[47] The mesh used for P3M was $64 \times 64 \times 64$.

The explicit consideration of the protein environment leads to an additional computational overhead of 60% with respect to standard CPMD calculations. This large computational demand limits the QM/MM simulations to a few picoseconds only.

TABLE 1: Interatomic Distances (Å) for Different QM and QM/MM Models[a]

distance (Å)	X-ray	model A_f	model A_c	model B	model C	model D	model 1	model 2
Zn1−Zn2	3.98	4.22	4.20	4.22	3.96	4.05	4.1 ± 0.1	4.1 ± 0.2
Zn1−Oc1	2.18	1.98	1.98	1.99	1.99	2.00	2.0 ± 0.1	2.0 ± 0.1
Zn1−Oc2	1.67	2.71	2.77	3.06	2.78	2.99	4.1 ± 0.1	3.2 ± 0.3
Zn1−Ob1	1.93	2.03	2.02		2.02	2.04	2.1 ± 0.1	2.0 ± 0.1
Zn1−Ob2	2.16	2.12	2.08		2.06	2.07	2.1 ± 0.1	2.1 ± 0.1
Zn1−Nδ1	1.94	2.09	2.05	2.01	2.05	1.98	2.1 ± 0.1	2.1 ± 0.2
Tyr-H···Oc2	2.25				1.82	1.75	1.9 ± 0.2	1.9 ± 0.2
His-Hϵ···Oa1	1.79			1.05		1.04	1.9 ± 0.1	1.8 ± 0.1
Zn2−Oc1	2.12	1.99	1.97	1.99	1.99	2.01	2.0 ± 0.1	2.0 ± 0.1
Zn2−Oc2	1.93	2.74	2.80	3.07	2.78	3.00	2.8 ± 0.3	2.8 ± 0.2
Zn2−Ob1	1.93	2.04	2.02	2.03	2.02	2.03	2.1 ± 0.1	2.1 ± 0.1
Zn2−Ob2	2.06	2.11	2.08	2.09	2.06	2.07	2.1 ± 0.1	2.1 ± 0.1
Zn2−Nδ2	2.00	2.08	2.06	2.00	2.05	1.98	2.1 ± 0.1	2.1 ± 0.1
Tyr-H···Oc2	3.03			1.05	1.82	1.74	1.9 ± 0.2	1.9 ± 0.2
His-Hϵ···Oa2	1.79					1.04	1.8 ± 0.1	1.9 ± 0.2

[a] The atom labeling scheme is reported in Figure 2.

3. Results and Discussion

Quantum Mechanical Calculations on Minimal Active Sites. As mentioned already, structural characterization of the enzyme mimic was performed using a series of first-principles calculations on different fragments of the active site. The starting point for the construction of the chosen fragments was the crystal structure of DF1.[14] As explained in the previous section, the simplest computational model (model A, Figure 2a) comprises the first shell ligands and the two zinc ions. To estimate the influence of structural constraints imposed by the four-helix bundle on the geometry of the active site, two simulations were performed with model A. In one case, the system was allowed to fully relax to a favorable equilibrium geometry (model A_f), while in the other case the terminal carbons were constrained to their crystallographic positions (model A_c). It is apparent from Table 1 that the presence of constraints only slightly influences the geometry of the active site. A decrease of only $\Delta d \sim 0.02$ Å in the distance between the transition metal atoms is observed in model A_c. Among the interatomic distances, Zn−Oc2 is the most sensitive to the presence of constraints ($\Delta d \sim 0.06$ Å). This confirms the previously observed flexibility[48−50] of the carboxylate (terminal or bridging) ligands that is expected to be a necessary condition to ensure structural stability and reactivity of the synthetic enzyme. The similar structural parameters of models A_c and A_f, along with a small difference in their relative thermodynamic stability ($\Delta E \sim 5$ kcal/mol), indicates that the steric constraints imposed by the four-helix bundle do not markedly affect the geometry of the active site. In addition, these results provide a qualitative indication that the first shell ligands strongly stabilize the doubly positively charged zinc ions.

Although only small structural and energetic differences are observed between models A_f and A_c, the latter provides a more realistic description of the active site; therefore, we compare its characteristic structural parameters with the crystal structure (Table 1).[14] A large increase of $\Delta d = 0.22$ Å (5% relative error) is observed in the Zn−Zn distance with respect to the X-ray structure. This large deviation is due mostly to the limited size of the computational model and partly to the limited accuracy of the X-ray structure.[51] Significant structural rearrangements of the chelating carboxylates were also observed. Contrary to the crystal structure, in which both oxygens bind to the active site, in this model only one oxygen (Oc1) binds to the central metal. As a result, both the terminal Glu residues are *syn*-monodentate.

As suggested experimentally,[14] second shell interactions play a key role in tuning the structural features of the active site. Therefore, model B also included the two aspartate residues that make hydrogen bonds to the His ligands. The addition of the second shell ligands does not affect the Zn−Zn distance ($d = 4.22$ Å). However, the Zn−Nδ bond length was shortened by $\Delta d = 0.04$ Å, due to the presence of the added aspartates. A substantial increase of the Zn−Oc2 distance occurs ($\Delta d \sim 0.30$ Å) with respect to model A_c. Evidently, the addition of the negatively charged Asp side chains induces an electrostatic repulsion toward other negatively charged Glu residues. This electrostatic repulsion, along with the large mobility of the terminal Glu, leads to a sensitive enlargement of the Zn−Oc2 distance. A surprising result obtained with model B is a transfer of the Hϵ of both histidine ligands to the Oa1 of the aspartates (His-Hϵ···Oa1−Asp = 1.05 Å). Histidine residues are expected to be neutral at physiological pH, although the pK_a of Hϵ might be lowered when the His ligands are coordinated to a transition metal. While unlikely in the real enzymatic system, this kind of proton transfer has previously been observed in gas phase models of active sites lacking the presence of an extended enzymatic and solvent environment.[52,53] The next section illustrates the crucial role played by the protein environment in stabilizing such hydrogen bond interaction.

In model C, different first and second shell interactions are taken into account, namely the hydrogen bonds between the chelating carboxylates and Tyr residues. The presence of these hydrogen bonds causes a contraction of the active site such that the Zn−Zn distance becomes $d = 3.96$ Å ($\Delta d \sim 0.02$ Å). Evidently, a Glu-Tyr interaction plays an important role in geometrically constraining the active site. A strong hydrogen bond is established between Tyr-H···Oc2 (1.82 Å), confirming the *syn*-monodentate coordination of the chelating Glu residues.

In the final purely QM model (model D), both the first and the second shell ligands considered earlier are included. As expected, this model, which encompasses all second shell interactions, leads to a short Zn−Zn distance ($d = 4.05$ Å, $\Delta d \sim 0.07$ Å and 2% relative error). Consistent with model B, the Zn−Oc2 bond length enlarges to $d \sim 3.00$ Å. An increase in the Zn−Oc2 interatomic distance of $\Delta d \sim 0.20$ Å with respect to model C also implies an increase of the Zn−Zn distance. Due to the structural rearrangement of Glu11 and Glu61, the Tyr-H···Oc2 hydrogen bonds become stronger (Hb ~ 1.75 Å, $\Delta d \sim 0.06$ Å with respect to model C). As in model B, a transfer of Hϵ of the His ligand to the aspartate side chain takes place. Thus, even a large QM model comprehensive of all first and second shell interactions (~100 atoms) does not necessarily

provide a good description of the active site of this enzyme, if the entire protein is neglected. The whole protein structure needs to be included in the calculations by performing hybrid QM/MM molecular dynamics simulations as described in the next section.

Hybrid QM/MM Calculations. In order to capture the biomimetic compound in its full complexity, a hybrid QM/MM approach was adopted. The starting point for the mixed quantum/classical calculations was the crystal structure of DF1 solvated with water molecules and previously equilibrated by performing classical molecular dynamics. As explained in the Computational Details section, two different partitioning schemes have been considered for these calculations.

Model 1 treats at a DFT level only the amino acid side chains that directly bind to the central metals. For this hybrid model, a short run of 3 ps was performed, 1 ps of which was for equilibration at room temperature. Average structural parameters are reported in Table 1. The Zn−Zn distance becomes ∼4.1 ± 0.1 Å, and consistent with the experimental Debye−Waller factors,[54] large thermal fluctuations are observed for the two transition metals. In addition, the two terminal carboxylate ligands are rather mobile, and in agreement with the pure QM calculations, they are both monodentate with a Zn−Oc1 average bond length of 2.0 ± 0.1 Å. This structural parameter is insensitive to the addition of the whole protein environment, while the Zn−Oc2 distance is affected considerably if the compound is considered in its full complexity. As reported in Table 1 and in Figure 4a, the two Zn−Oc2 interatomic distances are quite different in the two coordination spheres (Zn1−Oc2 ∼ 4.1 ± 0.1 Å and Zn2−Oc2 ∼ 2.9 ± 0.2 Å). The difference between the terminal carboxylates suggests that a large asymmetry is induced in the active site due to the presence of the protein environment, which leads to *syn*−*anti* isomerization for Glu11 already after 0.7 ps of simulation. In agreement with other theoretical data,[48] the *syn* coordination of carboxylates is usually favored with respect to the *anti*, but it has been shown that their relative thermodynamic stability is reduced if solvation and/or environmental effects are considered. Moreover, it has been recently demonstrated that *syn*/*anti* isomerization is likely to occur in carboxylate bridged binuclear proteins on the multi-picosecond time scale.[49] Therefore, it is likely that for long enough simulation times both *syn* and *anti* conformations will be sampled. Unfortunately, due to prohibitive computational cost, the present simulations span only a few picoseconds and are thus unlikely to sample many examples of such structural rearrangements.

The bridging carboxylates Glu37 and Glu87 are also mobile ligands, although they always maintain the μ-1,3-coordination mode. Large changes in the torsional angle defined by Zn1−Oδ2−Cγ−Oδ1 are observed during the molecular dynamics runs. By following this torsional angle for both bridging carboxylates, a substantial oscillatory motion is observed. However, while Glu87 performs relatively modest oscillations, assuming mostly positive values (30° ± 10°), Glu37 performs larger oscillations (−30° ± 30°). Due to this oscillatory motion, the two Zn−Ob1/Ob2 bonds assume identical average values for both bridging carboxylates (2.1 ± 0.1 Å).

In agreement with the QM calculations previously reported, the second shell ligands establish strong hydrogen bonds to the active site. The Tyr−Oc2 hydrogen bonds assume an average value of 1.9 ± 0.2 Å, for both coordination spheres. More sensitive is the hydrogen bond network involving the His-Hϵ···Oa1-Asp. Contrary to what was observed in the pure QM calculations, in the hybrid QM/MM calculations, the two

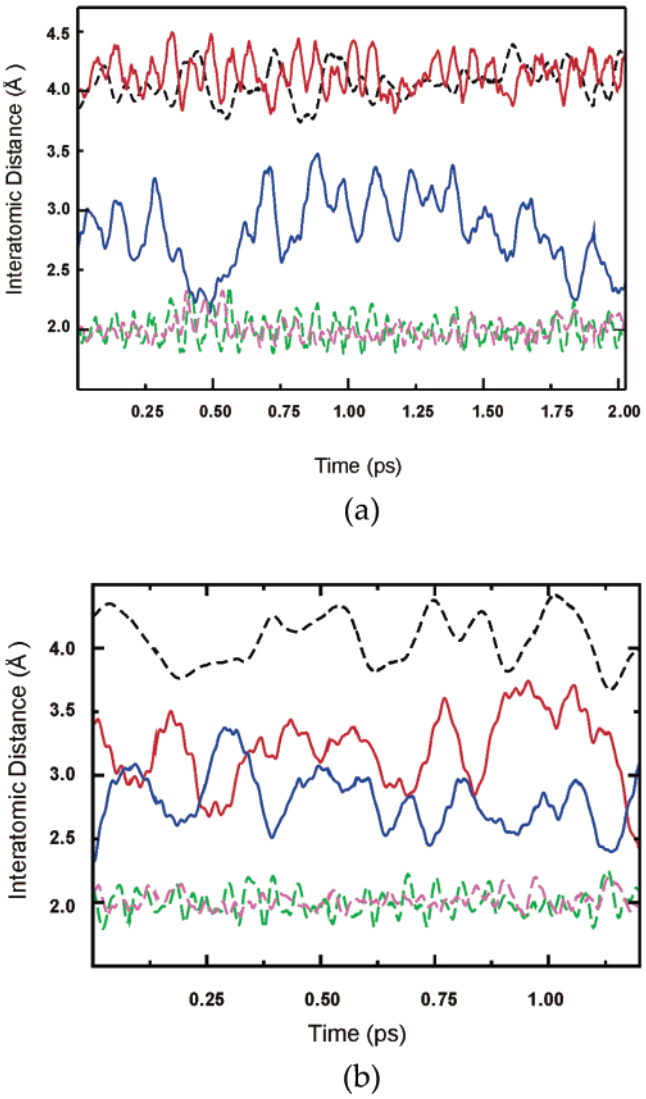

Figure 4. Selected interatomic distances as a function of simulation time for (a) model 1 and (b) model 2. The dashed line on the top represents the Zn−Zn separation; the red and the blue lines are the Zn−Oc2 distances for Glu11 and Glu61, respectively. The green and magenta dashed lines at the bottom are the Zn−Oc1 bond lengths for Glu11 and Glu61, respectively.

hydrogen bonds have an average length of ∼1.8 ± 0.1 Å and ∼1.9 ± 0.1 Å for His40, His90-Hϵ···Oa1-Asp, respectively. Interestingly, no proton transfer takes place.

However, with the QM/MM partitioning of model 1, all the second shell interactions are at the boundary region between the QM and the MM part. Although this model gives a good description of the hydrogen bond network,[55] it was considered worthwhile to verify the accuracy of this computational model with a second QM/MM partitioning in which the delicate His-Asp hydrogen bond network is fully treated at a QM level.

Starting from the same classically equilibrated structure used for model 1, a second QM/MM partitioning was adopted, in which both Asp36 and Asp86 were included in the QM region (Figure 3b). In addition, a direct comparison of different QM/MM partitioning schemes serves as a probe for the accuracy of the present computational approach. A short dynamics run of 1.5 ps was performed, of which 0.5 ps was equilibration. As shown by a comparison of the structural parameters in Table 1, large thermal fluctuations characterize the Zn−Zn distance that averages to a value 4.1 ± 0.2 Å (Figure 4b).

Surprisingly, a smaller asymmetry is observed for chelating carboxylates that coordinate both in a monodentate *syn* fashion. While the coordination average bond lengths are identical for the two coordination spheres (Zn−Oc1 ∼2.0 ± 0.1 Å), the Zn1,2−Oc2 distances are different and exhibit large fluctuations (Zn1−Oc2 ∼3.2 ± 0.3, Zn2−Oc2 ∼ 2.8 ± 0.2 Å). Although a small asymmetry is observed in model 2, Glu11 is again more weakly coordinated to the active site than Glu61. The different *anti*/*syn* coordination of Glu11 in models 1 and 2, respectively, may be attributed to a different equilibration time scale of the two hybrid models. As explained previously, the terminal carboxylates are quite flexible ligands, and for a longer dynamics run, it is likely that this structural rearrangement will take place several times for both models.

All the remaining ligands present very similar average bond lengths in the two QM/MM partitioning schemes. Each of the bridging carboxylates has Zn1,2−Ob1,2 ∼ 2.1 ± 0.1 Å due to oscillatory motion of the torsional angle Zn1−Ob2−Cγ−Ob1 (20° ±20°), while both Zn1,2−Nδ bond lengths average to 2.1 ± 0.1 Å. A comparison of the second shell interactions obtained from the two hybrid models is particularly interesting. The extended hybrid model leads to Tyr-H···Oc2-Glu hydrogen bonds (1.9 ± 0.2 Å) identical to the previous model. In good agreement with model 1, the full quantum mechanical description of the more critical His/Asp hydrogen bonds leads to His40-Hϵ···Oa1-Asp ∼ 1.8 ± 0.1 Å, His90-Hϵ···Oa1 ∼ 1.9 ± 0.2 Å. Therefore, no proton transfer occurs in the larger hybrid system, confirming that the proton transfer observed in the small QM models was caused by the lack of an extended protein environment. As shown in Figure 3b, the active site is not completely buried in the protein interior, and a hydrogen bond network exists that involves His and Asp residues, extending toward the solvent. This network strongly stabilizes the Asp negative charges so that the His-Hϵ···Oa1-Asp hydrogen bond can be adequately described only if the whole protein environment is considered. The hypothesis that the protein environment plays a crucial role in stabilizing hydrogen bond networks has often been suggested. However, the present work directly shows the role of the protein environment on second shell interactions. In addition, the agreement between the hydrogen bond His-Hϵ···Oa1-Asp described at the QM/MM boundary and fully at the QM-DFT level confirms the excellent quality of the present QM/MM approach.[45]

4. Conclusions

The structural and dynamical characteristics of a biomimetic enzyme, dizinc DF1, has been performed with pure QM and hybrid QM/MM (Car−Parrinello) molecular dynamics simulations. The use of minimal QM models indicates that a large electrostatic stabilization of the active site is provided by the six first shell ligands. In addition, second shell interactions contribute significantly to the structural stability of the active site. The steric restraint provided by the four-helix bundle is limited to only about 5 kcal/mol.

The effects of second shell hydrogen bonds are difficult to describe in the absence of an extended external environment. Calculations performed with the QM/MM models also show that second shell interactions must be involved in a hydrogen bond network linked to the bulk solvent water molecules in order to stabilize the active site. A large dynamical flexibility of the bridged carboxylate binuclear motif has been revealed in the molecular dynamics calculations, which involve the transition metals and both chelating carboxylate ligands. In QM/MM model 1, the highly flexible nature of the carboxylate bridged binuclear motif leads to a *syn*/*anti* isomerization of one terminal Glu residue. The excellent overall agreement between the average structural properties of the different QM/MM partitioning schemes confirms the accuracy of the present QM/MM computational approach[45] and its likely utility in aiding the design of future biomimetic proteins that exhibit catalytic activity.

The application of first-principles (Car−Parrinello) and hybrid QM/MM molecular dynamics simulations has been highly successful in providing a better understanding of the stability/reactivity governing factors of the carboxylate bridged binuclear motif. Therefore, in future work, we aim to investigate the dimanganese and diiron analogues of DF1 in order to explore and possibly improve their catalytic properties.

Acknowledgment. A.M. thanks the Swiss National Foundation for financial support during the initial stage of this research, which was also supported by the National Institutes of Health and the National Science Foundation. We are grateful to Ivaylo Ivanov, Petra Munih, and Simone Raugei for several useful discussions and Garegin Papoian for sharing his unpublished results.

References and Notes

(1) (a) Waller, B. J.; Lipscomb, J. D. *Chem. Rev.* **1996**, *96*, 2625. (b) Freig, A. L.; Lippard, J. D. *Chem Rev.* **1994**, *94*, 759.

(2) Lange, S. J.; Que, L. Jr. *Curr. Opin. Chem. Biol.* **1998**, **2**, 159.

(3) Stenkamp, R. E. *Chem. Rev.* **1994**, *94*, 715.

(4) (a) Powell, A. K. *Met. Ions. Biol. Syst.* **1998**, *35*, 515. (b) Harrison, P. M.; Hempstead, P. D.; Artymiuk, P. J.; Andrews, S. C. *Met. Ions. Biol. Syst.* **1998**, *35*, 435.

(5) Nordlund, P.; Eklung, H. *Curr. Opin. Struct. Biol.* **1995**, *5*, 758.

(6) (a) Gallagher, S. C.; George, A.; Dalton, H. *Eur. J. Biochem.* **1998**, *254*, 480. (b) Lee, M.; Lenman, M.; Banas, A.; Bator, M.; Singh, S.; Schweizer, N.; Nilsson, R.; Liljenberg, C.; Dahlquist, A.; Gummeson, P. D. *Science* **1998**, *280*, 915.

(7) (a) Nordlung, P.; Sjörberg, B. M.; Eklund, H. *Nature* **1990**, *345*, 593. (b) Bollinger, J. M. Jr.; Tong, W. H.; Ravi, N.; Huynh, B. H.; Edmondson, D. E.; Stubbe, J. A. *Methods Enzymol.* **1995**, *258*, 278.

(8) Shilov. A. E. *Activation of Saturated Hydrocarbons by Transition Metal Complexes*; D. Riedel Publishing Co.: Dordrecht, The Netherlands; 1984.

(9) Shilov, A. E.; Shul'pin, G. B. *Chem. Rev.* **1997**, *97*, 2879.

(10) (a) Lee, D.; Pierce, B.; Krebs, C.; Hendrich, M. P.; Huynh, B. H.; Lippard., S. J. *J. Am. Chem. Soc.* **2002**, *124*, 3993. (b) DuBois, J. D.; Mizoguchi, T. J.; Lippard, S. J. *Coord. Chem. Rev.* **2000**, *200*, 443.

(11) (a) Whittington, D. A.; Sazinsky, M. H.; Lippard, S. J. *J. Am. Chem. Soc.* **2001**, *123*, 1794. (b) Rosenzweig, A. C.; Brandstetter, H.; Whittington, D. A.; Nordlund, P.; Lippard, S. J.; Frederick, C. A. *Proteins* **1997**, *29*, 141.

(12) (a) Brazeau, B. J.; Austin, R. N.; Tarr, C.; Groves, J. T.; Lipscomb, J. D. *J. Am. Chem. Soc.* **2001**, *123*, 11831. (b) Brazeau, B. J.; Wallar, B. J.; Lipscomb, J. D. *J. Am. Chem. Soc.* **2001**, *123*, 10421.

(13) (a) Dunietz, B. D.; Beachy, M. D.; Cao, Y. X.; Whittington, D. A.; Lippard, S. J.; Friesner, R. A. *J. Am. Chem. Soc.* **2000**, *122*, 2828. (b) Guallar, V.; Gherman, B. F.; Miller, W. H.; Lippard, S. J.; Friesner., R. A. *J. Am. Chem. Soc.* **2002**, *124*, 3377. (d) Guallar, V.; Gherman, B. F.; Lippard, S. J.; Friesner, R. A. *Curr. Opin. Struct. Biol.* **2002**, *6*, 236. (e) Torrent, M.; Vreven, T.; Musaev, D. G.; Morokuma, K.; Farkas, O.; Schlegel. H. B. *J. Am. Chem. Soc.* **2002**, *124*, 192. (f) Musaev, D. G.; Basch, H.; Morokuma. K. *J. Am. Chem. Soc.* **2002**, *124*, 4135. (g) Siegbahn. P. E. M. *Chem. Phys. Lett.* **2002**, *351*, 311. (h) Siegbahn., P. E. M. *J. Am. Chem. Soc.* **1998**, *120*, 8417. (i) Siegbahn, P. E. M.; Blomberg, M. R. A. *J. Am. Chem. Soc.* **1997**, *119*, 3103.

(14) Lombardi, A.; Summa, C. M.; Geremia, S.; Randaccio, L.; Pavone, V.; DeGrado, W. F. *Proc. Natl. Acad. Sci. U.S.A.* **2000**, *97*, 6298.

(15) Di Costanzo, L.; Wade, H.; Geremia, S.; Randaccio, L.; Pavone, V.; DeGrado, W. F.; Lombardi, A. *J. Am. Chem. Soc.* **2001**, *123*, 12749.

(16) Summa, C. M.; Lomardi, A.; Lewis, M.; DeGrado, W. F. *Curr. Opin. Struct. Biol.* **1999**, *9*, 500.

(17) Lawson, D. M.; Artymiuk, P. J.; Yewdall, S. J.; Smith, J. M.; Livingstone, J. C.; Treffry, A.; Luzzago, A.; Levi, S.; Arosio, P.; Cesarini, G. Thomas, C. D.; Shaw, W. V.; Harrison, P. M. *Nature* **1991**, *349*, 541.

(18) Frolow, F.; Kalb, A. J.; Yariv, J. *Nat. Struct. Biol.* **1994**, *1*, 453.

(19) (a) deMare, F.; Kurtz, D. M.; Nordlund, P. *Nat. Struct. Biol.* **1996**, *3*, 539. (b) Sieker, L. C.; Holmes, M.; Le Trong, I.; Truly, S.; Santarsiero, B. D.; Liu, M. Y.; LeGall, J.; Stenkamp, R. E. *Nat. Struct. Biol.* **1999**, *6*, 308.

(20) Lindqvinst, Y.; Huang, W.; Schneider, G.; Shanklin, J. *EMBO J.* **1996**, *15*, 4081.

(21) Wilcox, D. E. *Chem. Rev.* **1996**, *96*, 2435−2458. (b) Lipscomb, W. N.; Sträter, N. *Chem. Rev.* **1996**, *96*, 2375.

(22) Wilce, M. C. J.; Bond, C. S.; Dixon, N. E.; Freeman, H. C.; Guss, J. M.; Lilley, P. E.; Wilce, J. A. *Proc. Natl. Acad. Sci. U.S.A.* **1998**, *95*, 3472.

(23) Liu, S.; Widom, J.; Kemp, C. W.; Crews, C. M.; Clardy, J. *Science* **1998**, *282*, 1324.

(24) Dismukes, G. C. *Chem. Rev.* **1996**, *96*, 2909.

(25) Barynin, V. V.; Whittaker, M. M.; Antonyuk, S. V.; Lamzin, V. S.; Harrison, P. M.; Artymiuk, P. J.; Whittaker. J. W. *Structure* **2001**, *9*, 725.

(26) Antonyuk, S. V.; Melik-Adamyan, V. R.; Popov, A. N.; Lamzin, V. S.; Hempstead, P. D.; Harrison, P. M.; Artymiuk, P. J.; Barynin, V. V. *Crystallogr. Rep. (Transl. Kristallografiya)* **2000**, *45*, 105.

(27) Ash, D. E.; Cox, J. D.; Christianson, D. W. *Met. Ions Biol. Syst.* **2000**, *37*, 407.

(28) Högbom, M.; Andersonn, M. E.; Nordlung, P. *J. Bioinorg. Chem.* **2001**, *6*, 315.

(29) Car, R.; Parrinello, M. *Phys. Rev. Lett*. **1985**, *55*, 2471.

(30) (a) Carloni, P.; Rothlisberger, U. *Theoretical and Computational Chemistry*; Eriksonn, L. A., Ed.; Elsevier: New York, 2001; Vol. 9, Chapter 6, p 215. (b) Gao, J.; Thompson, M. A. *Combined quantum mechanical and molecular mechanical methods*; ACS Symposium Series 712; American Chemical Society: Washington, DC, 1998. (c) Agarwal, P. K.; Billiter, S. R.; Hammes-Schiffer, S. *J. Phys. Chem. B* **2002**, *106*, 3283. (d) Agarwal, P. K.; Billiter, S. R.; Rajagopalan, P. T. R.; Benkovic, S. J.; Hammes-Schiffer, S. *Proc. Natl. Acad. Sci. U.S.A.* **2002**, *99*, 2749.

(31) Marx, D.; Hutter, J. *Modern Methods and Algorithms of Quantum Chemistry*; Grotendorst, J., Ed.; John von Neumann Institute for Computing Juelich, NIC Series; 2000; Vol. 1, p 301.

(32) Hutter, J.; Alavi, A. Deutsch, T.; Ballone, P.; Bernasconi, M.; Focher, P.; Goedecker, S.; Tuckerman, M.; Parrinello, M. *CPMD*; Max-Planck-Institut für Festkörperforschung: Stuttgart, and IBM Research Laboratory: Zürich, 1995−1999.

(33) Trouiller, N.; Martins, J. L. *Phys. Rev. B* **1991**, *43*, 8861.

(34) Kleinmann, L.; Bylander, D. M. *Phys. Rev. Lett.* **1982**, *48*, 1425.

(35) Rothlisberger, U. *ACS Symp. Ser.* **1998**, *712*, 264.

(36) Gervasio, F. L.; Schettino, V.; Mangani, S.; Kranc, M.; Carloni, P.; Parrinello, M. *J. Phys. Chem. B*, submitted.

(37) Dal Peraro, M.; Villa, A. J.; Carloni, P. *J. Biol. Inorg. Chem.* **2002**, *7*, 704−712.

(38) Becke, A. D. *Phys. Rev. A* **1988**, *38*, 3098.

(39) Lee, C.; Yang, W.; Parr, R. G. *Phys. Rev. B* **1988**, *37*, 785.

(40) Carloni, P.; Rothlisberger, U. In *Theoretical biochemistry—processes and properties of biological systems*; Eriksonn, L., Ed; Elsevier: Amsterdam, 2001; pp 215−252.

(41) Hockney, R. W. *Methods Comput. Phys.* **1970**, *9*, 136.

(42) Rothlisberger, U. To be published.

(43) Pearlman, D. A.; Case, D. A.; Caldwell, J. W.; Ross, W. S.; Cheatham, T. E.; Debolt, S.; Ferguson, D.; Seibel, G.; Kollman, P. *Comput. Phys. Commun.* **1995**, *91*, 1.

(44) Ryckaert, J. P.; Ciccotti, G.; Berendsen, H. J. C. *J. Comput. Chem.* **1997**, *23*, 327.

(45) Laio, A.; VandeVondele, J.; Rothlisberger, U. *J. Chem. Phys.* **2001**, *116*, 6941.

(46) The so-called spill-out effect refers to an unphysical escape of electron density from the QM to the MM atoms.

(47) Hünenberger, P. *J. Chem. Phys.* **2000**, *113*, 10464.

(48) Ryde, U. *Biophys. J.* **1999**, ***77***, 2777.

(49) Papoian, G.; DeGrado, W. F.; Klein, M. L. *J. Am. Chem. Soc.* **2003**, *125*, 560.

(50) Torrent, M.; Musaev, D. G.; Morokuma, K. *J. Phys. Chem. B* **2001**, *105*, 322.

(51) The resolution of the crystal structure used as a starting point for our calculations is only 2.5 Å. Therefore, an uncertainty of 0.2−0.3 Å can be expected in the structural parameters.

(52) Dudev, T.; Lim, C. *J. Phys. Chem. B* **2001**, *105*, 4446.

(53) Lovell, T.; Li, J.; Noodleman, L. *Inorg. Chem.* **2001**, *40*, 5251.

(54) Large *B* factors are observed for all atoms in the X-ray structure. In particular, the two Zn ions show a *B* factor of 30 Å^2. This becomes even larger for the two terminal carboxylate ligands (40 Å^2), while the two bridging carboxylates have a *B* factor of 30 Å^2.

(55) At the interface between the QM and MM region, no proton transfer is expected to occur. The inadequate description of the hydrogen bonds is indicated by an inappropriate elongation of the His-Hϵ bond.